Anomalous Fluctuations in a Droplet of Chemically Active Colloids or Enzymes

K. R. Prathyusha,[1,2,3,*] Supriya Saha,[1,2,*] and Ramin Golestanian[1,2,4,†]
[1]Max Planck Institute for Dynamics and Self-Organization (MPI-DS), D-37077 Göttingen, Germany
[2]Max Planck Institute for Physics of Complex Systems, Dresden, Germany
[3]School of Chemical and Biomolecular Engineering, Georgia Institute of Technology, Atlanta, Georgia 30332, USA
[4]Rudolf Peierls Centre for Theoretical Physics, University of Oxford, Oxford OX1 3PU, United Kingdom

(Received 25 January 2024; accepted 28 June 2024; published 30 July 2024)

Chemically active colloids or enzymes cluster into dense droplets driven by their phoretic response to collectively generated chemical gradients. Employing Brownian dynamics simulation techniques, our study of the dynamics of such a chemically active droplet uncovers a rich variety of structures and dynamical properties, including the full range of fluidlike to solidlike behavior, and non-Gaussian positional fluctuations. Our work sheds light on the complex dynamics of the active constituents of metabolic clusters, which are the main drivers of nonequilibrium activity in living systems.

DOI: 10.1103/PhysRevLett.133.058401

Introduction—The nonequilibrium physical rules that determine the behavior of active matter [1] can naturally be expected to provide clues towards unraveling the spatiotemporal self-organization observed in living systems. In particular, biochemical reactions facilitated by enzyme molecules and metabolic activity make the interior of a cell a nonequilibrium environment with persistent chemical gradients and fluxes [2,3]. Theories of active phase separation, describing the phase behavior of motile or living units, incorporate, in addition to thermodynamic fluxes, particle currents stemming from nonequilibrium interactions, some examples of which are chemical interactions [4–12], quorum sensing [13,14], nonreciprocity [15–17], and catalysis [18].

Inside living cells, the structural compartmentalization of biomolecules in the form of droplets are thought to help their function, such as regulating biochemical processes [19,20]. These condensates are typically in a dynamic liquid-like state, although they can also exhibit solidlike properties when associated with pathological conditions [21,22]. Because of the metastable nature of the liquidlike assemblies, they also exist in glassy or gel-like states that do not have the properties of a classical liquid [23]. For instance, *in vitro* tracer diffusion measurements within phase-separated droplets have shown caging and other signatures of glassy behavior [24], while metabolic activity of bacteria has been shown to affect the diffusivity of the proteins within the cell cytoplasm [25,26].

Despite an overwhelming wealth of empirical observations, the interplay between enzymatic activity in the cytosol and the fluidity of protein condensates is still not understood from a mechanistic perspective. The nonequilibrium phoretic interactions, which naturally arise from chemical activity [27], have the potential to play a major role in such a regulation mechanism, in the same vein as the recently proposed mechanisms that may have led to the self-organization of metabolic cycles during the early stages of life formation [28–30].

Here, we explore the complex dynamics within a droplet formed by long-ranged phoretic interaction between chemically active colloids or enzymes. Tracking the motion of a tagged biomolecule provides information about the dynamics and structure inside a droplet [see Figs. 1(a)–1(c)]. The

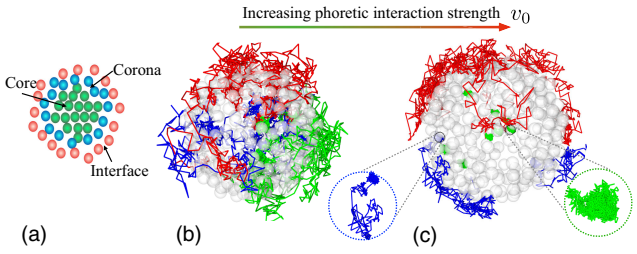

FIG. 1. (a) A schematic showing different regions—core, corona, interface—in a cross section of a cluster. (b) Trajectories of tagged colloids in a fluidlike cluster (weak phoretic interaction) are superimposed on transparent particles. A tagged particle travels freely throughout the entire cluster, see Supplemental Material, movie SM1 [31]. (c) In an arrested cluster (strong phoretic interaction), particle tracks vary qualitatively depending on their initial location in the cluster. Completely trapped colloids (green track), and those that exhibit several cage breaking events (red and blue tracks) are seen in the same time window; see Supplemental Material, movie SM2 [31].

*These authors contributed equally to this work.
†Contact author: ramin.golestanian@ds.mpg.de

Published by the American Physical Society under the terms of the Creative Commons Attribution 4.0 International license. Further distribution of this work must maintain attribution to the author(s) and the published article's title, journal citation, and DOI. Open access publication funded by the Max Planck Society.

series of structural changes, which occur as the dimensionless coupling strength v_0 is increased, is accompanied by dramatic changes in the dynamics of a single particle (see Figs. 2 and 3). The chemotactic collapse is cutoff by steric repulsion, and the cluster undergoes a gradual transition from a fluidlike state (see Supplemental Material, movie SM3 [31]) to a solidlike state (see Supplemental Material, movie SM7 [31]) as v_0 is increased. At intermediate values of v_0 (see Supplemental Material, movies SM4–6 [31]), the cluster develops a solid core surrounded by a relatively mobile region that we call the corona, which in turn is followed by an interface consisting of chemically active colloids that are nearly free [see Fig. 1(a)]. Using the distribution of the positional fluctuations calculated as a function of the step size and initial location of the colloid as our main tool, we probe the glassy dynamics in this mesoscopic droplet and provide several experimentally testable results.

Theoretical model—We consider N active colloids of radius σ within a spherical container of radius R, with the stochastic trajectory of the ith particle $(i = 1, \ldots, N)$ denoted as $\boldsymbol{r}_i(t)$. Each active colloid catalyzes a chemical reaction converting a reactant, assumed to be abundantly available, into a product at a rate α. They generate a chemical field $c(\boldsymbol{r}, t)$ at position $\boldsymbol{r}$ that evolves following the diffusion equation with sources at $\boldsymbol{r}_i$, namely, $\partial_t c - D_c \nabla^2 c = \alpha \sum_i \delta(\boldsymbol{r} - \boldsymbol{r}_i)$, where D_c is the diffusion coefficient of the chemicals. Imposing the boundary condition $c(|\boldsymbol{r}| = R, t) = 0$ ensures that the chemicals are continuously generated in the container and extracted at the boundary, hence creating a nonequilibrium steady state. Variation of c on the colloid surface establishes a diffusiophoretic slip velocity and thus net drift with a velocity $-\mu \boldsymbol{\nabla} c$, where μ is the diffusiophoretic mobility (that is negative for attractive phoretic interactions) [27]. The equation of motion of the ith colloid is given as $\dot{\boldsymbol{r}}_i = -\mu \boldsymbol{\nabla} c(\boldsymbol{r}_i, t) + \sum_{i \neq j} v(r_{ij}) \hat{\boldsymbol{r}}_{ij} + \boldsymbol{\zeta}_i$, where $\boldsymbol{r}_{ij} = \boldsymbol{r}_i - \boldsymbol{r}_j$, $r_{ij} = |\boldsymbol{r}_{ij}|$ and $\hat{\boldsymbol{r}}_{ij} = \boldsymbol{r}_{ij}/r_{ij}$. $v(r_{ij}) = 24\epsilon[2(2\sigma)^{12} r_{ij}^{-13} - (2\sigma)^6 r_{ij}^{-7}]$ is a derivative of the Weeks-Chandler-Anderson potential [33]. It imposes steric repulsion between the colloids and vanishes for $r_{ij} > 2^{1/6}(2\sigma)$. The parameter ϵ combines the strength of repulsion and the viscous damping and is kept constant at unity. The random fluctuations are included through the white noise term, $\boldsymbol{\zeta}$, with zero mean and intensity $2D$, where D is the thermal diffusivity of the colloids.

Assuming a separation of scale between the sizes of the chemicals and the colloids, we can use the quasi-stationary solution for c since $D \ll D_c$. Moreover, we use the far-field approximation [11,34] and ignore corrections due to the proximity of colloids. This approximation is justified since exact solutions have shown that near-field effects are unimportant for exactly similar active colloids [35]. With these approximations, the chemical gradient $\boldsymbol{\nabla} c$ can be determined explicitly as a function of colloid positions $\boldsymbol{r}_i$ as follows

$$\boldsymbol{\nabla} c(\boldsymbol{r}_i, t) = \frac{\alpha}{4\pi D_c} \left[\sum_{j \neq i}^{N} \frac{\boldsymbol{r}_{ij}}{r_{ij}^3} - \sum_{j=1}^{N} \frac{(R/r_j)\boldsymbol{r}'_{ij}}{r'^3_{ij}} \right], \tag{1}$$

Where $\boldsymbol{r}'_{ij} = \boldsymbol{r}_i - (R^2/r_j^2)\boldsymbol{r}_j$, $r'_{ij} = |\boldsymbol{r}'_{ij}|$ and $r_j = |\boldsymbol{r}_j|$. Scaling position by σ and time by σ^2/D, we identify a dimensionless constant $v_0 = |\mu|\alpha/(DD_c\sigma)$ which determines the strength of the interactions with respect to the fluctuations.

Particle trajectories are obtained by the Euler integration of the dynamics with a time step $\Delta t = 0.001$. The data presented in this Letter are for $N = 1000$ unless otherwise specified. The value of v_0 varies between 0.5 and 5.0. The colloids assemble to form a single spherical droplet of size equal to a few colloidal radii ($\sim 10\sigma$) at the center of the confining sphere due to the long-range interaction between them.

Self-part of the Van Hove functions—The central result of our work is the analysis of anomalous fluctuations to illustrate several aspects of the dynamics that follow from the chemically mediated long-range interactions. We do so by calculating the self-part of the Van-Hove functions (SVH) [36]. In a fluid with no internal structure [37], the SVH is Gaussian, while in a supercooled fluid it is Gaussian with exponential tails [38,39]. We calculate the SVH by *distinguishing* the initial position of the colloid in the droplet. As a result the distribution depends on whether the colloids were located initially in the frozen core or the corona. The self part of the Van-Hove function $G(x, \tau)$ is defined as follows:

$$G(x, \tau) = \frac{1}{n} \sum_{i=1}^{n} \langle \delta(x - [x_i(\tau + t) - x_i(t)]) \rangle. \tag{2}$$

$G(x, \tau)$ is the probability distribution function that a colloid traverses a displacement x in an interval of time τ. Variation of $G(x, \tau)$ with the waiting time τ provides information about the changing neighborhood of a colloid. The τ dependent step size is thus simply the distance $x_i(t + \tau) - x_i(t)$, where the time t is chosen large enough such that the cluster has reached a steady state. In the definition (2), the index i is used to average over a total of n number of colloids which are at time t located in a particular shell from the center of mass of the cluster (as shown schematically in Fig. 2). Since G is identical for fluctuations in the three orthogonal directions, we present an average over all three directions.

We find that G reveals a wealth of information about the spatial dependence of structural rearrangements within the cluster when it is calculated for those located in the core, the corona, or the interface. For small v_0, G is well approximated by a Gaussian irrespective of the initial

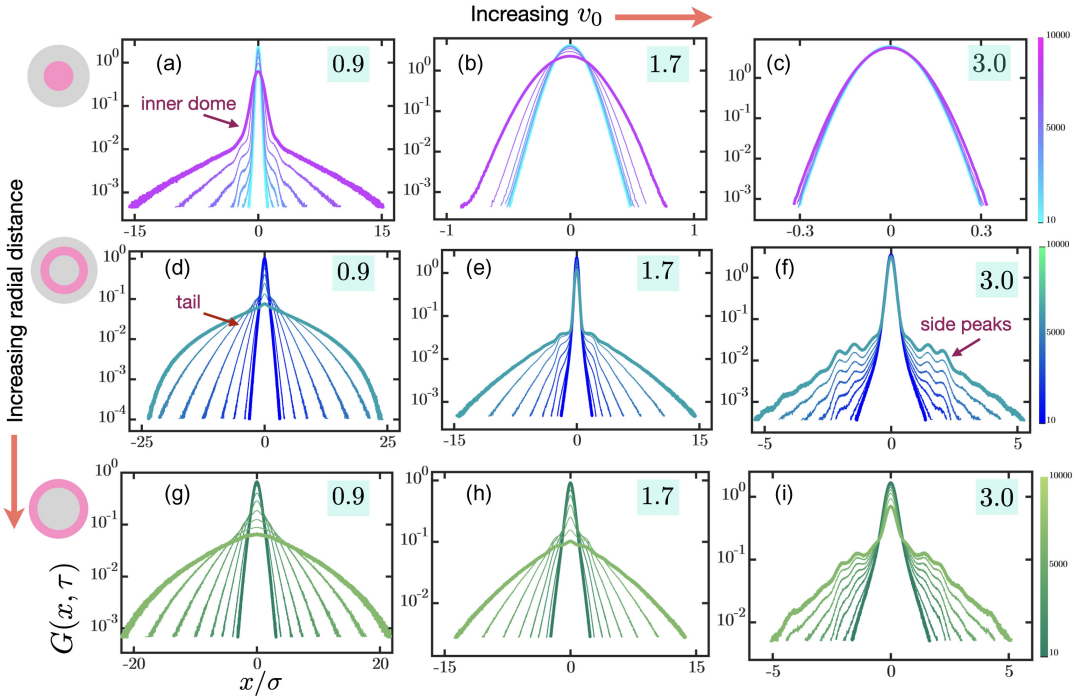

FIG. 2. Self-part of the Van Hove function (probability distribution of colloidal displacements). $G(x,\tau)$ in a partly arrested droplet is shown for a different values of v_0 (as indicated), increasing from left to right. G for colloids initially located within a distance of $3-6\sigma$ (core), $6-9\sigma$ (corona), and $9-12\sigma$ (interface) of the center, are plotted in the three rows (from top to bottom) as indicated with illustrations. The color maps, which indicate the waiting time τ, are chosen to be the same for colloids belonging to the same region in the cluster. A peak at $x=0$, indicative of a colloid trapped in a cage, is always present for colloids that are initially located in the core, as seen in panels (a)–(c). Such a peak is absent in fluids, and reveals slow relaxation. The peak is less pronounced for colloids originating in the corona [see in panels (d)–(f)], and vanishes completely for those that start in the interface [see (g)–(i)]. Those in panels (d)–(i) show pronounced tails extending until $\sim 10\sigma$. At $v_0=3.0$ fluctuations with magnitude of the order a few σ show secondary peaks mirroring the structure formation, as seen in panels (f) and (i).

location of the colloids, and its width increases as $\sim\sqrt{\tau}$ for all τ. For a value of v_0 for which the cluster is close to the solid state, G begins to show signatures of trapping at small τ, and cage-breaking dynamics at larger values of τ. Calculated for colloids in the core with initial positions within $3-6\sigma$ from the centre of the cluster, G shows a sharp peak at $x=0$ as seen in Figs. 2(a)–2(c). The unimodal graph falls sharply within $x\sim\sigma$ showing that the colloids in the interior of the cluster for $v_0=1.7$ are caged by their neighbors [see Figs. 2(b) and 2(c)]. For colloids initially located in the corona within 6–9σ from the center, the distribution clearly develops a tail—which broadens with increasing τ [see Figs. 2(d)–2(f)]. For colloids with initial locations in the interface within 9–12σ, G shows tails whose widths increase with increasing τ [Figs. 2(g)–2(i)]. Thus the dynamics varies greatly from the center to the surface—the innermost colloids vibrate in nearly permanent cages (over the time scale of the simulations), the ones which are in the corona are trapped for variable duration of time and released before they are trapped again. Colloids at the interface typically make long excursions [Figs. 2(g)–2(i)]. In the fully arrested state, G shows a single peak at $x=0$ of nearly constant width for all τ [Figs. 2(c), 2(f), and 2(i)]. Deep into the solid state fluctuations close to $x=0$ develop additional features such as secondary peaks that reflect the underlying positional order [Figs. 2(f) and 2(i)]. Such side peaks have been reported in other active matter systems due to the action of molecular motors in a gel [40].

To elucidate the non-Gaussian nature of the fluctuations, we fit the inner dome and the outer tail of G to a family of curves called the q Gaussian [41,42], which provides a framework to describe systems with long-range interactions [43] (see Supplemental Material for details [31]). The q-Gaussian of a length x scaled by ℓ is $[1-(1-q)(x/\ell)^2]^{[1/(1-q)]}$. In general, the range of the exponent q is $-\infty<q<3$, approaching the Gaussian as $q\to 1$. For $q<1$, the domain of the function is bounded, i.e., $-1<x/\ell<1$, while for $q>1$, x/ℓ is unbounded. G calculated for colloids in the core is well fitted by the $q=1.45$, corresponding to strong correlations [44]. For G calculated for those in the corona, the tail is fitted by $0<q<1$. A fitted value of q smaller than unity suggests that fluctuations smaller than a length scale are suppressed. We also calculate the distribution of time intervals between successive cage-breaking events. The distribution changes

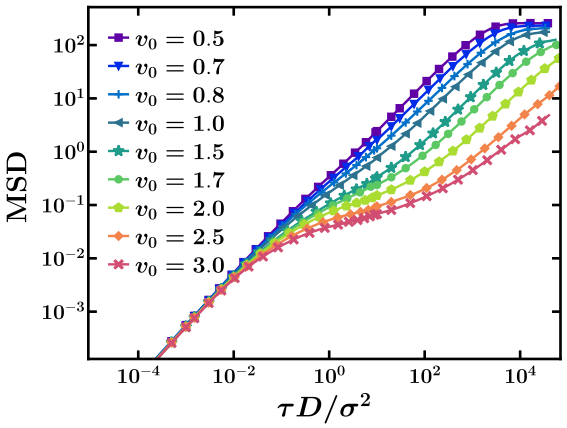

FIG. 3. Mean square displacement (MSD) for different values of v_0. A plateau develops in the arrested states as colloids are repeatedly trapped into, and released from temporary cages. The reduction in the MSD upon increasing v_0 is due to the increase in the attractive interaction between colloids, and saturation corresponds to the cluster size.

from being exponential in the fluid state to a power law in the solid (see Supplemental Material for details [31]).

Mean square displacement—We discuss fluctuations in colloid position as captured by calculating the mean square displacement (MSD) for all colloids in the droplet (see Supplemental Material for MSD calculated by distinguishing the initial location of the colloids [31]). The center of mass of the mesoscopic cluster diffuses while it also rotates as a whole. To measure relative displacements of particles, we transform to a body-fixed frame of reference located at the center of the cluster using methods described in [45]. The MSD is calculated by averaging over trajectories of all particles as $\mathrm{MSD}(t) = N^{-1}\sum_{i=1}^{N}\langle|\mathbf{r}_i(t) - \mathbf{r}_i(0)|^2\rangle$, and shown in Fig. 3, for v_0 in the range 0.5–3.0. A plateau, defined as a flattening of the MSD curve after an initial diffusive regime is visible at sufficiently large values of v_0, and is particularly prominent in the arrested state. It emerges as the colloids get trapped or caged by their neighbors and spend a long time inside those cages. Such a subdiffusive plateau is a signature of the motion of active particles in a complex and crowded environment [46], in contrast to a freely moving active particle. The trapped colloids escape from their cages after a timescale that increases with increasing v_0, as apparent in Fig. 3. Note that the trapping occurs at comparable timescales ($\sim\tau$) in all v_0s but in contrast, escape from a cage is a collective maneuver and the related timescale increases over 3 orders of magnitude from the fluid to the solid state.

State diagram—We construct a state diagram by varying both v_0 and the total number of particles. Using cues from both the arrangement of colloids within the droplet and their dynamics, we identify two stages in between the fluidlike and the solidlike droplet which are called "lamellar" and "lamellar-with-core" [see Fig. 4(c)]. Periodic deviations around the smooth radial density profile,

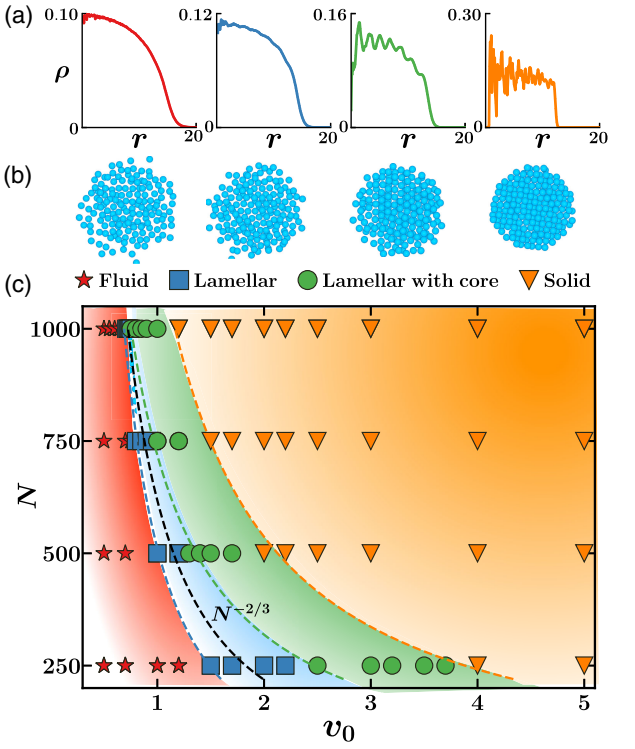

FIG. 4. (a) Density profile for $v_0 = 0.5$, 0.7, 0.9, 3.0 corresponding to states fluid, lamellar, lamellar-with-core, and solid, respectively. (b) Snapshots from simulations illustrating typical structure of the droplet in each state. (c) State diagram in the $N - v_0$ plane, showing fluid, lamellar, lamellar-with-core, and arrested states. Note that the state boundaries shift towards smaller values of v_0 with increasing system size. The dashed black line is the power-law scaling expected using a scaling argument (see Appendix).

calculated from the center of mass of the droplet, serves as the metric to distinguish a *lamellar droplet* that has developed shells like an onion from a fluidlike droplet without spatial ordering [see Figs. 4(a) and 4(b) and Supplemental Material for details [31]]. The dynamics in a lamellar droplet is still fluidlike (Supplemental Material, movie SM4 [31]). Development of structural inhomogeneities in a similar density of the positions of colloids within a spherical shell at an even higher v_0 signals the transformation of a lamellar droplet into a lamellar droplet with a core. In the state lamellar-with-core, the droplet develops an inner core within which colloids are immobile due to the surrounding dynamic layer that we call the corona [see Figs. 4(a) and 4(b), Supplemental Material, movies SM5 and SM6 [31]]. Irregular sharp peaks in densities reveal that the solid structure formed is not isotropic due to the finite size of the cluster [see Figs. 4(a) and 4(b) and Supplemental Material for details and Supplemental Material, movie SM7 [31]]. Figure 4(c) displays a state diagram in the $N - v_0$ plane and shows that the state boundaries shift to lower values of v_0 with increasing N, which is a feature of the long-range

interactions mediated by the chemical field. The transition from fluid to solid occurs when v_0 is large enough to drive an instability analogous to gravitational collapse, beyond a threshold $v_0 \sim N^{-2/3}$ [4] (see Appendix for the derivation of the scaling argument).

Concluding remarks—The strength of the effective interaction mediated by the collective response of the colloids to the chemical field determines whether the cluster resembles a fluid or is rather in a hybrid state with a central core resembling a solid and an outer corona of relatively freely moving colloids. We observe strikingly different dynamics in the two cases: in the first case, the colloids are free to span the full cluster while the motion of the caged ones is restricted to a fraction of the colloids in the second case. We observed narrow Gaussian peaks and extended tails in the distributions of particle displacements, similar to what is ubiquitously observed in glassy systems [38,39,47], where the dominant dynamics of the particles is random hopping and trapping, also including solid-liquid interfaces [48]. The crucial difference between the system at hand and the classically studied systems is that in our system both the inner dome and the tail are fitted by the q-Gaussian.

Finally, we note that the exponent of anomalous diffusion, and the parameter q quantifying the degree of nonextensivity are related in simple systems via the Tsallis-Bukman law [49], which has been verified experimentally in vibrated granular rods [50]. In the present case, the finite size of the droplet leads to the formation of a layered inhomogeneous structure with an interface that give rise to a relatively more complex dynamics with q exponents that depend on the waiting time, and continuously time-varying anomalous exponent (scaling of the MSD). Therefore, we do not expect such a simple relation to hold here, as any given trajectory will effectively sample different types of environment governed by different statistical properties in each short segment of the dynamics (see Ref. [31] for details). Our results will be helpful to serve as a motivation for further theoretical developments that are needed to characterize cage-breaking dynamics in a finite active inhomogeneous cluster.

Acknowledgments—We thank J. Agudo-Canalejo, A. Amiri, B. Mahault, Y. Pollack, S. Rulands, A. Vilfan, F. Ziebert, and D. Zwicker for useful discussions. R. G. acknowledges a Martin Gutzwiller Fellowship of the Max Planck Institute for the Physics of Complex Systems in Dresden. This work has received support from the Max Planck School Matter to Life and the MaxSyn-Bio Consortium, which are jointly funded by the Federal Ministry of Education and Research (BMBF) of Germany, and the Max Planck Society. We acknowledge the use of the Max Planck Computing and Data Facility (MPCDF) in Garching.

[1] G. Gompper *et al.*, The 2020 motile active matter roadmap, J. Phys. Condens. Matter **32**, 193001 (2020).
[2] G. M. Cooper, *The Cell: A Molecular Approach. 2nd Edition* (Sinauer Associates, Sunderland, MA, 2000).
[3] A. Testa, M. Dindo, A. A. Rebane, B. Nasouri, R. W. Style, R. Golestanian, E. R. Dufresne, and P. Laurino, Sustained enzymatic activity and flow in crowded protein droplets, Nat. Commun. **12**, 6293 (2021).
[4] R. Golestanian, Collective behavior of thermally active colloids, Phys. Rev. Lett. **108**, 038303 (2012).
[5] J. Palacci, S. Sacanna, A. P. Steinberg, D. J. Pine, and P. M. Chaikin, Living crystals of light-activated colloidal surfers, Science **339**, 936 (2013).
[6] O. Pohl and H. Stark, Dynamic clustering and chemotactic collapse of self-phoretic active particles, Phys. Rev. Lett. **112**, 238303 (2014).
[7] B. Liebchen, D. Marenduzzo, I. Pagonabarraga, and M. E. Cates, Clustering and pattern formation in chemorepulsive active colloids, Phys. Rev. Lett. **115**, 258301 (2015).
[8] D. Zwicker, A. A. Hyman, and F. Jülicher, Suppression of Ostwald ripening in active emulsions, Phys. Rev. E **92**, 012317 (2015).
[9] D. Zwicker, R. Seyboldt, C. A. Weber, A. A. Hyman, and F. Jülicher, Growth and division of active droplets provides a model for protocells, Nat. Phys. **13**, 408 (2017).
[10] R. Golestanian, Division for multiplication, Nat. Phys. **13**, 323 (2016).
[11] J. Agudo-Canalejo and R. Golestanian, Active phase separation in mixtures of chemically-interacting particles, Phys. Rev. Lett. **123**, 018101 (2019).
[12] J. Bauermann, G. Bartolucci, J. Boekhoven, C. A. Weber, and F. Jülicher, Formation of liquid shells in active droplet systems, Phys. Rev. Res. **5**, 043246 (2023).
[13] M. E. Cates and J. Tailleur, Motility-induced phase separation, Annu. Rev. Condens. Matter Phys. **6**, 219 (2015).
[14] T. Bäuerle, A. Fischer, T. Speck, and C. Bechinger, Self-organization of active particles by quorum sensing rules, Nat. Commun. **9**, 3232 (2018).
[15] S. Saha, J. Agudo-Canalejo, and R. Golestanian, Scalar active mixtures: The nonreciprocal Cahn-Hilliard model, Phys. Rev. X **10**, 041009 (2020).
[16] Z. You, A. Baskaran, and M. C. Marchetti, Nonreciprocity as a generic route to traveling states, Proc. Natl. Acad. Sci. U.S.A. **117**, 197767 (2020).
[17] S. Osat and R. Golestanian, Non-reciprocal multifarious self-organization, Nat. Nanotechnol. **18**, 79 (2023).
[18] M. W. Cotton, R. Golestanian, and J. Agudo-Canalejo, Catalysis-induced phase separation and autoregulation of enzymatic activity, Phys. Rev. Lett. **129**, 158101 (2022).
[19] A. A. Hyman, C. A. Weber, and F. Jülicher, Liquid-liquid phase separation in biology, Annu. Rev. Cell Dev. Biol. **20**, 39 (2014).
[20] B. Niebel, S. Leupold, and M. Heinemann, An upper limit on Gibbs energy dissipation governs cellular metabolism, Nat. Metab. **1**, 125 (2019).
[21] S. Alberti and A. A. Hyman, Biomolecular condensates at the nexus of cellular stress, protein aggregation disease and ageing, Nat. Rev. Mol. Cell Biol. **22**, 197 (2021).
[22] Y. Shin and C. P. Brangwynne, Liquid phase condensation in cell physiology and disease, Science **357**, 1253 (2017).

[23] D. T. Murray, M. Kato, Y. Lin, K. R. Thurber, I. Hung, S. L. McKnight, and R. Tycko, Structure of fus protein fibrils and its relevance to self-assembly and phase separation of low-complexity domains, Cell **171**, 615 (2017).
[24] L. Jawerth, E. Fischer-Friedrich, S. Saha, J. Wang, T. Franzmann, X. Zhang, J. Sachweh, M. Ruer, M. Ijavi, S. Saha, J. Mahamid, A. A. Hyman, and F. Jülicher, Protein condensates as aging Maxwell fluids, Science **370**, 1317 (2020).
[25] B. R. Parry, I. V. Surovtsev, M. T. Cabeen, C. S. O'Hern, E. R. Dufresne, and C. Jacobs-Wagner, The bacterial cytoplasm has glass-like properties and is fluidized by metabolic activity, Cell **156**, 183 (2014).
[26] N. Bellotto, J. Agudo-Canalejo, R. Colin, R. Golestanian, G. Malengo, and V. Sourjik, Dependence of diffusion in *Escherichia coli* cytoplasm on protein size, environmental conditions, and cell growth, eLife **11**, e82654 (2022).
[27] R. Golestanian, Phoretic active matter, in *Active Matter and Nonequilibrium Statistical Physics: Lecture Notes of the Les Houches Summer School: Volume 112, September 2018* (Oxford University Press, New York, 2022).
[28] V. Ouazan-Reboul, J. Agudo-Canalejo, and R. Golestanian, Self-organization of primitive metabolic cycles due to non-reciprocal interactions, Nat. Commun. **14**, 4496 (2023).
[29] V. Ouazan-Reboul, R. Golestanian, and J. Agudo-Canalejo, Network effects lead to self-organization in metabolic cycles of self-repelling catalysts, Phys. Rev. Lett. **131**, 128301 (2023).
[30] V. Ouazan-Reboul, R. Golestanian, and J. Agudo-Canalejo, Interaction-motif-based classification of self-organizing metabolic cycles, New J. Phys. **25**, 103013 (2023).
[31] See Supplemental Material at http://link.aps.org/supplemental/10.1103/PhysRevLett.133.058401, which includes Ref. [32], for details on the numerical simulations, the measures used to determine the phase boundaries and quantitative analysis of the non-Gaussian fluctuations.
[32] J. Helfferich, F. Ziebert, S. Frey, H. Meyer, J. Farago, A. Blumen, and J. Baschnagel, Continuous-time random-walk approach to supercooled liquids. I. Different definitions of particle jumps and their consequences, Phys. Rev. E **89**, 042603 (2014).
[33] J. D. Weeks, D. Chandler, and H. C. Andersen, Role of repulsive forces in determining the equilibrium structure of simple liquids, J. Chem. Phys. **54**, 5237 (1971).
[34] R. Soto and R. Golestanian, Self-assembly of catalytically active colloidal molecules: Tailoring activity through surface chemistry, Phys. Rev. Lett. **112**, 068301 (2014).
[35] B. Nasouri and R. Golestanian, Exact phoretic interaction of two chemically active particles, Phys. Rev. Lett. **124**, 168003 (2020).
[36] L. Van Hove, Correlations in space and time and born approximation scattering in systems of interacting particles, Phys. Rev. **95**, 249 (1954).
[37] J.-P. Hansen and I. R. McDonald, *Theory of Simple Liquids: With Applications to Soft Matter* (Elsevier/AP, Amstersdam, 2013).
[38] P. Chaudhuri, L. Berthier, and W. Kob, Universal nature of particle displacements close to glass and jamming transitions, Phys. Rev. Lett. **99**, 060604 (2007).
[39] E. R. Weeks, J. C. Crocker, A. C. Levitt, A. Schofield, and D. A. Weitz, Three-dimensional direct imaging of structural relaxation near the colloidal glass transition, Science **287**, 627 (2000).
[40] E. Ben-Isaac, E. Fodor, P. Visco, F. van Wijland, and N. S. Gov, Modeling the dynamics of a tracer particle in an elastic active gel, Phys. Rev. E **92**, 012716 (2015).
[41] C. Tsallis, Possible generalization of Boltzmann-Gibbs statistics, J. Stat. Phys. **52**, 479 (1988).
[42] G. Wilk and Z. Włodarczyk, Interpretation of the nonextensivity parameter q in some applications of Tsallis statistics and Lévy distributions, Phys. Rev. Lett. **84**, 2770 (2000).
[43] C. Tsallis, Non-additive entropies and statistical mechanics at the edge of chaos: A bridge between natural and social sciences, Phil. Trans. R. Soc. A **381**, 20220293 (2023).
[44] U. Tirnakli, M. Marques, and C. Tsallis, Entropic extensivity and large deviations in the presence of strong correlations, Physica (Amsterdam) **431D**, 133132 (2022).
[45] G. L. Hunter, K. V. Edmond, M. T. Elsesser, and E. R. Weeks, Tracking rotational diffusion of colloidal clusters, Opt. Express **19**, 17189 (2011).
[46] C. Bechinger, R. Di Leonardo, H. Löwen, C. Reichhardt, G. Volpe, and G. Volpe, Active particles in complex and crowded environments, Rev. Mod. Phys. **88**, 045006 (2016).
[47] W. K. Kegel, van Blaaderen, and Alfons, Direct observation of dynamical heterogeneities in colloidal hard-sphere suspensions, Science **287**, 290 (2000).
[48] M. J. Skaug, J. Mabry, and D. K. Schwartz, Intermittent molecular hopping at the solid-liquid interface, Phys. Rev. Lett. **110**, 256101 (2013).
[49] C. Tsallis and D. J. Bukman, Anomalous diffusion in the presence of external forces: Exact time-dependent solutions and their thermostatistical basis, Phys. Rev. E **54**, R2197 (1996).
[50] G. Combe, V. Richefeu, M. Stasiak, and A. P. F. Atman, Experimental validation of a nonextensive scaling law in confined granular media, Phys. Rev. Lett. **115**, 238301 (2015).

End Matter

Appendix: The scaling argument from a continuum theory—We have outlined an argument for determining the boundaries separating various states in Fig. 4. In this Appendix, we present a coarse-grained description for the time evolution of the number density ρ of the colloids as coupled to the concentration c of the substrate, and sketch the steps that lead us to the derivation of the scaling law. Averaging over thermal noise, we define the mean number density by summing over the positions $\boldsymbol{r}_i$ of the individual colloids as $\rho(\boldsymbol{r},t)=\sum_i\langle\delta(\boldsymbol{r}-\boldsymbol{r}_i)\rangle$. Ignoring the short-range repulsive interactions between the colloids, we can derive [4] the dynamics for ρ as

follows:

$$\partial_t \rho = D\nabla^2 \rho + \mu \boldsymbol{\nabla} \cdot (\rho \boldsymbol{\nabla} c), \tag{A1}$$

where c is the concentration field produced collectively by the colloids and D is the variance of the thermal noise in the Langevin dynamics of a single colloid. The concentration c is governed by the following reaction-diffusion equation

$$\partial_t c - D_c \nabla^2 c = \alpha \rho. \tag{A2}$$

Following the same approximations as in the main text, i.e., a separation of timescales between the diffusion of the chemicals and the diffusion of the colloids, we can formally solve for the chemical concentration field as follows:

$$c = \frac{\alpha}{D_c} \int \mathrm{d}^d \boldsymbol{r}' \mathcal{G}(\boldsymbol{r} - \boldsymbol{r}') \rho(\boldsymbol{r}'), \tag{A3}$$

where $\mathcal{G}$ is the Green's function described in the main text that implements the boundary condition of vanishing flux on the surface of the confining sphere. Substituting the expression for c in Eq. (A1) we obtain the effective equation for ρ as

$$\partial_t \rho(\boldsymbol{r}, t) = D\nabla^2 \rho - \frac{\mu\alpha}{D_c} \boldsymbol{\nabla} \cdot \left[\rho \boldsymbol{\nabla} \int \mathrm{d}^d \boldsymbol{r}' \mathcal{G}(\boldsymbol{r} - \boldsymbol{r}') \rho(\boldsymbol{r}') \right]. \tag{A4}$$

From Eq. (A4), it is clear that the cluster is formed by a competition between the first and the second terms which describe respectively diffusion and attractive effective interactions between the colloids, which correspond to the case where μ is negative. Writing the density as $\rho(\boldsymbol{r}, t) = \rho_0 + \delta\rho(\boldsymbol{r}, t)$, in terms of a mean uniform density ρ_0 and density fluctuations $\delta\rho(\boldsymbol{r}, t)$, we can perform a linear stability analysis of the homogeneous state in Fourier space $\boldsymbol{q}$ and approximately implement the finite size of the cluster via a minimum cutoff on $|\boldsymbol{q}|$. We obtain $\partial_t \delta\rho(\boldsymbol{q}, t) = \lambda(\boldsymbol{q}) \delta\rho(\boldsymbol{q}, t)$, where the growth rate is given as

$$\lambda(\boldsymbol{q}) = -D\boldsymbol{q}^2 + \alpha|\mu|\rho_0 / D_c. \tag{A5}$$

We observe that (for negative μ) $\lambda(\boldsymbol{q})$ is positive for all perturbations with wave numbers $|\boldsymbol{q}| < q_0$, where $q_0 = \sqrt{\alpha|\mu|\rho_0/(DD_c)} = \sqrt{v_0\rho_0\sigma}$, signaling a system-wide instability. To obtain a critical value of v_0 we stipulate that the transition from fluid to solid occurs when $q_0 \approx L^{-1}$, where L is the minimum size of a close-packed cluster, such that $L^3 \approx \sigma^3 N$, which yields the scaling relation

$$v_0 \propto \sigma^2 / L^2 \propto N^{-2/3}. \tag{A6}$$

Following [4] we can formulate an alternative argument for the derivation of the scaling relation from the stability of steady-state profiles of the chemical field c. At steady state, where the phoretic drift flux balances the diffusive flux, Eqs. (A1) and (A2) can be combined to obtain a Poisson-Boltzmann-type equation for $\tilde{c} = |\mu| c / D$ (the nondimensionalized chemical concentration)

$$-\nabla^2 \tilde{c} = k^2 \exp(\tilde{c}), \tag{A7}$$

where $k^2 = 4\pi\alpha\mu\rho_0/(DD_c) = 4\pi v_0 \sigma \rho_0$, which is the same combination of terms that appears in Eq. (A5). As discussed in [4], the density of c at the middle of the cluster grows with increasing k^2 until the outgoing flux at the boundary can no longer balance the phoretic fluxes leading to a collapse. The condition for collapse depends on the dimension, and in three dimensions is given by $N v_0 \sigma / L = \text{const}$. Substituting $L^3 \approx \sigma^3 N$ as the critical size when the collapse occurs, we find that v_0 at the transition scales as $N^{-2/3}$ identical to the arguments based on linear stability analysis of the homogeneous state.